Effective Diffusivity in Porous Media under Rarefied Gas Conditions

V. Casseau and C. White[a)]

School of Engineering, University of Glasgow, Glasgow G12 8QQ, UK

[a)]Corresponding author: craig.white.2@glasgow.ac.uk

Abstract. For future space missions in which soft landings on extra-terrestrial bodies will be required, it is important to understand the interaction of the propulsion system with the surface of the body. During the landing phase, the porous surface regolith can become contaminated with the exhaust products of the rocket plume, and this contamination must be minimised if sample return from the landing site is the goal of the mission. How far in-depth the exhaust products can reach depends on the effective diffusivity of the gas in the porous surface regolith material. The purpose of this work is to study the influence of temperature, gas number density, and adsorption parameters on the effective diffusivity in highly porous media under rarefied conditions. The procedure to recover the effective diffusivity, using direct simulation Monte Carlo, from a real sample is presented, along with trends as parameters are being varied, which will prove informative for later use of simplified engineering methodologies that assume a homogeneous porous structure.

INTRODUCTION

For future space missions in which soft landings on extra-terrestrial bodies will be required, *e.g.* [1], it is important to understand the interaction of the propulsion system with the surface of the body. During the landing phase, the porous surface regolith can become contaminated with the exhaust products of the rocket plume. For a sample return mission, it is necessary to minimise the degree of contamination in the collected soil so that it can be analysed reliably upon return. In the case of a body with a thin atmosphere, the in-depth penetration can be thought of as gas particles from a rarefied exhaust plume impinging inside the pores of the regolith; essentially the problem of a rarefied gas passing through a porous medium.

How far into the regolith the exhaust products can reach depends on the effective diffusivity of the gas in the material. Effective diffusivity describes diffusion through the pore space of a porous media and is a macroscopic property because it is measured over the whole pore space. In this work, the direct simulation Monte Carlo (DSMC) technique [2] is employed to measure the effective diffusivity of a gas in porous media. The geometries considered are highly porous and either generated from micro-computed tomography (μCT) scans, or randomly from a python script.

METHODOLOGY

The direct simulation Monte Carlo method

The DSMC method is a particle-based methodology that is prominently used in modelling flows under rarefied gas conditions. DSMC simulators each represent a large number of real molecules/atoms and are moved ballistically, while collision events are treated stochastically after the movement step, thus making the DSMC algorithm tractable across a wide range of Knudsen numbers ranging from the continuum-slip regime to the free-molecular regime. This work makes use of the open-source *dsmcFoam+* [3] solver that is available at [4].

Effective diffusivity computation

Here, *dsmcFoam+* is extended with measurement functions suitable for porous media. The effective diffusivity of the gas, D_{eff}, is calculated by measuring the mean squared displacement of the DSMC simulators in the domain using the Einstein equation [5, 6]. The definition of the mean squared displacement, MSD, for a particle cloud of size N is written

$$MSD(t) = \frac{1}{N} \sum_{p=1}^{N} \left\| \mathbf{r}_p(t) - \mathbf{r}_p(t_0) \right\|^2, \tag{1}$$

where $\mathbf{r}_p$ denotes the position of the particle p in a 3D Cartesian coordinate system and t_0 refers to the time at which all particles are to be tracked from. It follows that

$$D_{\text{eff}}(t) = \frac{MSD(t)}{2\,q\,(t - t_0)}, \tag{2}$$

where q is the dimensionality of the problem (*e.g.*, 1 for a one-dimensional case). The time evolution of the mean squared displacement of a diffusion-driven gas in an open-space configuration follows the trend shown in Figure 1. After a sufficient amount of particle collision events, a linear trend is observed and this constant rate of increase in MSD is used for the computation of the effective diffusivity while benchmarking *dsmcFoam+*.

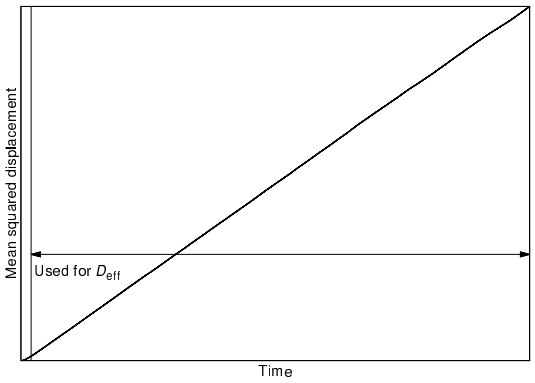

FIGURE 1. Mean squared displacement versus time for a diffusion-driven open-space configuration (*dsmcFoam+*).

Surface mechanisms modelling

The approach retained for modelling the adsorption and desorption mechanisms is described in [7] and the code has been further developed to include temperature- and species-dependent sticking probabilities as well as a local saturation limit. Models chosen in this study are voluntarily simplistic and described below.

Adsorption

When a DSMC simulator strikes an adsorbing wall, it has a probability equal to $\mathcal{P}_{\text{ads}}$ of being adsorbed, and a probability $1 - \mathcal{P}_{\text{ads}}$ of undergoing a diffuse reflection. To decide on the type of interaction, $\mathcal{P}_{\text{ads}}$ is compared to a randomly generated scalar ranging between 0 and 1, designated by $\Re_{\text{ads}}$. If $\mathcal{P}_{\text{ads}} > \Re_{\text{ads}}$, the simulator is adsorbed by the wall by being fully accommodated to the surface temperature, and having its velocity components set to zero.

Desorption

An adsorbed particle is considered for release if the ratio of the simulation time-step to the adsorption residence time, τ_{ads}, is greater than another randomly generated scalar $\Re_{\text{des}}$. The new particle velocity is sampled from a Maxwellian distribution function.

Saturation

The amount of contamination already bounded to the surface is considered via an adsorption saturation limit, $\mathcal{S}_{\text{ads}}$ in particles m^{-2}, defined as the product of the adsorption saturation limit fraction by the number of available sites for chemical bounding on a 1 m^2 sticking surface. As a result, an additional condition must be fulfilled for a molecule to be adsorbed; $\mathcal{N}_{\text{ads},f} < \mathcal{S}_{\text{ads}}\mathcal{A}_f$, where the subscript f refers to the boundary face hit by the simulator and $\mathcal{A}_f$ and $\mathcal{N}_{\text{ads},f}$ are the face area and number of molecules currently adsorbed on that face, respectively.

Porous media mesh generation

Generation from micro-CT scans

Numerical meshes can be generated from μCT scans of real porous media, as described in [8]. A three-dimensional representation of the pore arrangement within the material can be extracted and further processed to obtain a castellated mesh similar to the one shown in Figure 2(a). Simulating the entire original sample is computationally intractable, hence sub-samples are randomly extracted (see Figure 2(b)) and two mesh sizes are selected for this investigation: 40×40×40 voxels (in green) and 80×80×80 voxels (in red). To decide on the number of subsamples to extract, the mean porosity is plotted in Figure 2(c) as the subsample collection increases in size. Covering 20 % of the μCT scan volume in subsamples allows for the sampled porosity to fall within 1 % of the overall porosity of the material sample. The subsample porosity distribution at this 20 % mark is given in Figure 2(d) and as expected it is less spread out for the larger mesh size with nearly 85% of the subsamples porosity falling in the 0.80–0.90 band. Mean porosity, μ, and standard deviation, σ, are given in this Figure. These give a 95% confidence interval of 0.8517-0.8763 and 0.8504-0.8715 for the 80×80×80 and 40×40×40 subsamples, respectively. For comparison, the measured porosity of the entire μCT scan is 0.855. These results show that taking a small subsample from a large μCT scan of a highly porous material is unlikely to give a porosity and tortuosity that is representative of the entire material and that a large number of subsamples must be extracted in order to have a representative study.

Random generation

The intricate arrangement of porous media necessitates different levels of idealisation when it comes to numerical modelling without real-world inputs [9] and random generation is an attractive choice due to its relatively simplistic implementation. A python script has been written to generate random 3D porous media according to a user-defined porosity and the output can be read by OpenFOAM to create a castellated mesh. It is ensured that there are no closed cavities, *i.e.*, that all pores are interconnected. The present analysis is limited to random 2D porous media and therefore, interconnection between all solid regions is neither needed nor enforced. After prescribing the domain size and the resolution, the user chooses the elementary solid shapes as well as their sizing factor from which the algorithm is going to perform a random selection. In the following, the investigation is restricted to a cubic shape of size equal to the resolution, while other pre-defined patterns might have been utilised as well to alter the pore size. A typical grid thus being generated is presented in Figure 3.

RESULTS

Verification and validation

This subsection aims at showing the correct implementation of the features described in the methodology using (a) a zero-dimensional heat bath and (b) a single-cell simulation with one sticking wall for the surface mechanisms feature.

Heat bath

Firstly, a heat bath is utilised to determine the self-diffusion coefficient of argon at standard temperature and pressure (STP) conditions. Indeed, in the present case $D_{\text{eff}} = D_{11}$ and the code developments presented therein can thus be used for this purpose. The single cell of length 1×10^{-5} m is filled with argon at a temperature of 273 K and the reference number density, n_{Ar}, is set to 1.4×10^{22} m^{-3}. Since the diffusion coefficient scales with the inverse of the number density, D_{eff} at STP conditions can be recovered by multiplying the computed value by the factor $\frac{n_{Ar}}{n_{Lo}}$, where $n_{Lo} = 2.687 \times 10^{25}$ m^{-3} is the Loschmidt number. All boundaries are set to be specular walls and the time-step is set to 1×10^{-9} s. The experimental value of D_{eff} reported by Chapman and Cowling [10] is 1.57×10^{-5} m^2 s^{-1}. In addition,

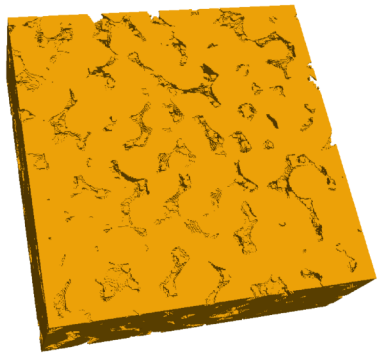

(a) Numerical mesh obtained after processing a mixed ceramic foam μCT scan (porosity: 0.855, resolution: 36 μm, ~ 50M voxels). The fluid region is visualised.

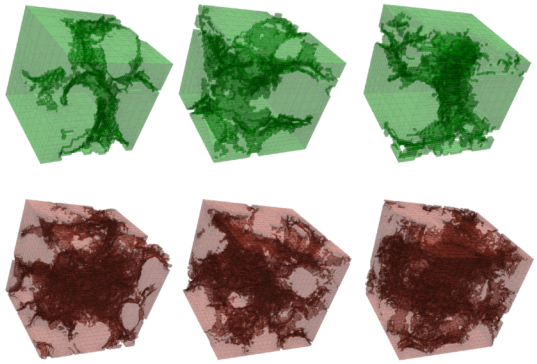

(b) Randomly-selected subsamples extracted from the original sample. In green: 40×40×40 voxel grids, in red: 80×80×80 voxel grids.

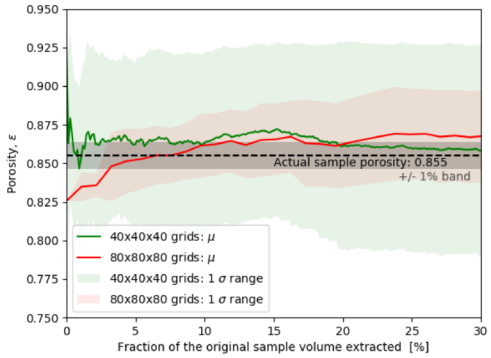

(c) Evolution of the mean porosity with subsample size.

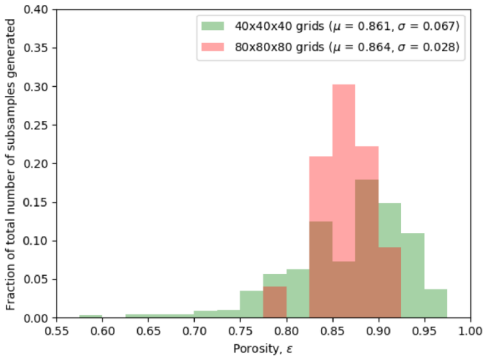

(d) Subsample porosity distribution.

FIGURE 2. Porous medium mesh generation from a μCT scan and presentation of the criteria to make an informed choice on the number of subsamples to collect.

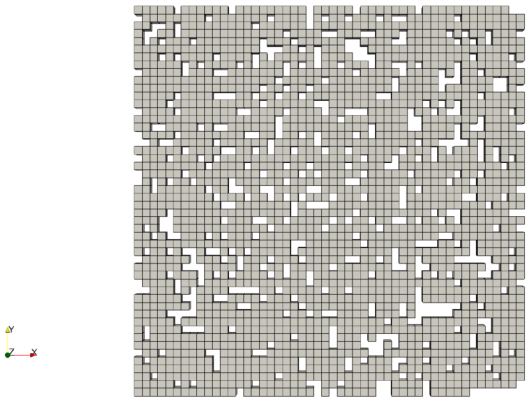

FIGURE 3. Example of a randomly generated porous medium mesh with no closed pores (porosity: 0.8, resolution: 36 μm). The visible part represents the fluid region.

Bird [2] performed a DSMC computation of a 1-D channel where argon was being injected at both ends. Variable soft sphere (VSS) argon particles entering through the left patch were assigned the label 1, while those coming in

through the right patch were marked with a label equal to 2. The simulation was run until steady-state and was then time-averaged. Letting $n_{\text{mix}} = n_{Ar_1} + n_{Ar_2}$, and using the following equation for the diffusion coefficient

$$D_{12} = D_{11} = (U_{Ar_2} - U_{Ar_1}) \frac{n_{Ar_1} n_{Ar_2}}{n_{\text{mix}}^2} \nabla \left(\frac{n_{Ar_1}}{n_{\text{mix}}} \right), \tag{3}$$

where U_{Ar} is the mean velocity of the argon gas, and the average value over the 1-metre long channel was found to be 1.55×10^{-5} m^2 s^{-1}.

In Figure 4(a), D_{eff} is shown to be in good agreement with those two references with a value close to 1.54×10^{-5} m^2 s^{-1}. Figure 4(b) shows a time history of the effective diffusivity as calculated from the mean squared displacement. This *dsmcFoam+* computation was repeated twice, increasing the argon number density by a factor 10 and 100, and as was expected the value of D_{eff} at STP conditions was not affected by this change. Furthermore, a heat bath simulation using $n_{Ar} = 1.4 \times 10^{22}$ m^{-3} is finally re-run for a variable hard sphere (VHS) gas (which is equivalent to a VSS gas with $\alpha = 1$), and a VSS gas with $\alpha = 1.67$, the value prescribed by Koura and Matsumoto [11]. As anticipated, the effective diffusivity is proportional to $\alpha + 1$ and the linear regression is shown in Figure 4(a).

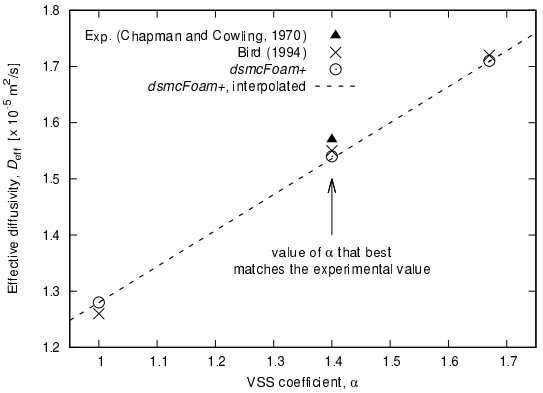

(a) Self-diffusion of argon versus α for the heat bath simulation.

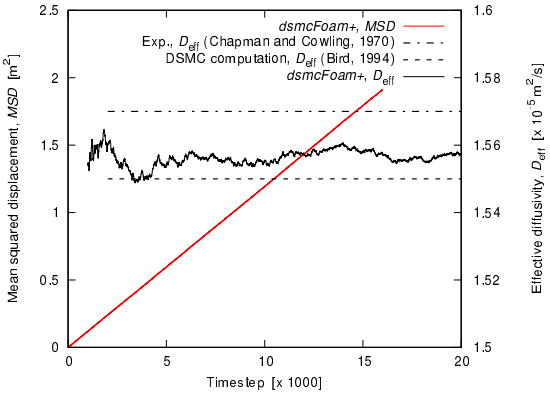

(b) Mean squared displacement and effective diffusivity history for the 1-D cyclic channel simulation of a VSS (α = 1.4) argon gas.

FIGURE 4. Effective diffusivity computations in *dsmcFoam+* and comparison with experimental data and Bird's computations.

Sticking wall

A single cubic cell case scenario is selected again, with the edge length set to 1×10^{-5} m. Argon with number density equal to 1×10^{21} m^{-3} is at a temperature of 2000 K within the box. The number of real atoms represented by each DSMC simulator, denoted by F_N, is taken as 100. All boundaries are set to be walls and as such, the number of DSMC simulators within the box remains constant with time. Five faces are specularly reflective, with the final boundary assigned to be a mixed sticking/diffusive wall. On the mixed patch the striking particles are fully accommodated to the wall temperature of 2000 K. Finally, the time-step is set to 1×10^{-9} s and the DSMC simulation is run for 1000 iterations.

Effects of the residence time and saturation limit are disregarded in the first computation that is tagged Run 1 in Figure 5(a) and in which $\mathcal{P}_{\text{ads}} = 0.5$. Editing the adsorbing wall patch to account for the desorption mechanism, an artificial residence time of $\tau_{\text{ads}} = 5 \times 10^{-8}$ s is set in the simulation tagged Run 2 and the simulation outcome is shown to be in agreement with the analytical solution given in [12]. The saturation limit entry is considered in Run 3 and for the sake of example, say there cannot be more than $N_{\text{max}} = 2000$ DSMC parcels (*i.e.* 20 % of the total number of DSMC parcels) stuck on that wall. Then, *dsmcFoam+* should be provided with a fictitious adsorption saturation limit given by the following relationship:

$$\mathcal{S}_{\text{ads}} = \frac{N_{\text{max}} \times F_N}{\mathcal{A}_f} = \frac{2000 \times 100}{1 \times 10^{-10}} = 2.0 \times 10^{15} \text{ particles m}^{-2}. \tag{4}$$

The time history of the number of stuck atoms for Run 3 is shown in Figure 5(b) using a solid green line. The desired goal of having a maximum of 20 % of the total number of DSMC parcels bounded to the wall is met.

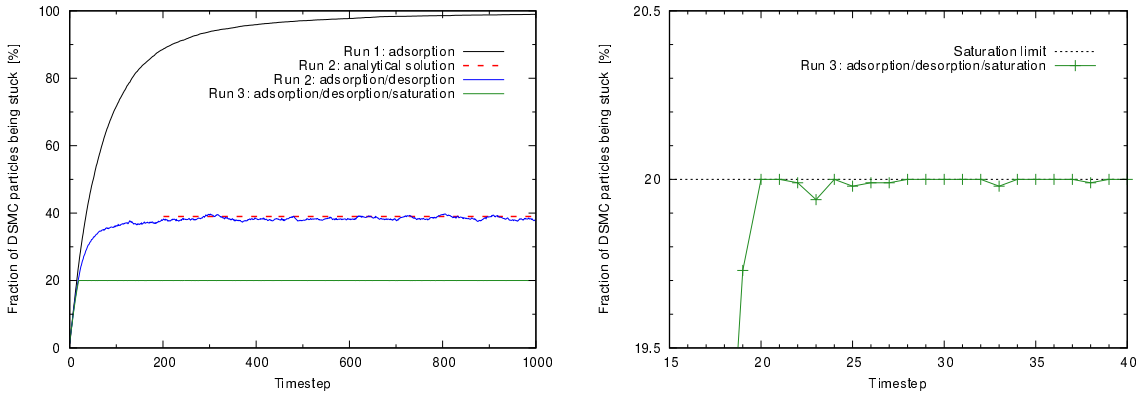

(a) Full time history.

(b) First 40 timesteps for Run 3.

FIGURE 5. Adsorption, desorption and saturation phenomena on a sticking DSMC patch.

Application to porous media

Porous media of interest to this work belongs to the class of foams, such as the alumina foam, Al_2O_3, or mixed ceramic foams. They are highly porous with porosities typically spanning from 0.8 to 0.9. In the subsequent simulations, the default configuration features argon as a working VSS gas and the initial temperature and number density are set to be 273 K and 1.4×10^{20} m^{-3}, respectively. Using the resolutions of 36 μm as the minimum pore size and characteristic length, the Knudsen number is 257, *i.e.* free-molecular flow. The domain boundaries are specular walls, while the solid surfaces are diffusely reflective with full thermal accommodation and a temperature of 273 K. A time-step of 1×10^{-7} s is retained and 50000 time steps are used.

Micro-CT scan

The different subsamples generated from the μCT scans in the Methodology section are simulated using the working gas described above and the effective diffusivity is derived for each run and denoted by a symbol in Figure 6. The mean and standard deviation of this population gives a 95% confidence interval of 0.06174-0.07341 m^2 s^{-1} for the 80×80×80 samples and 0.0624-0.0991 m^2 s^{-1} for the 40×40×40 samples. It is evident that that even for similar porosities, there can be a large range of effective diffusivity due to the different tortuosity values for each subsample, which again highlights the importance of performing many small simulations (when it is intractable to perform a single large simulation) in order to obtain a result that is more representative of the material.

Random porous media

The python script inputs detailed in the Methodology are adopted and 10 independent generations are run for each porosity so as to obtain a solution that has reduced dependence on any specific mesh features that would result from the random generation. Effects of temperature, number density, and surface mechanism parameters of adsorption probability, residence time and saturation limit on D_{eff} are shown in Figure 7. At high porosities, there are clear differences in the effective diffusivity for a given temperature and number density, indicating that the tortuosity of the individual randomly generated geometries has an influence on the effective diffusivity and so care must be taken to either average over multiple geometries or use a much larger mesh. It can be noted that the trend in D_{eff} when varying the porosity alone is similar to the one shown for the mixed ceramic foam μCT scan. For the parameter space explored, the gas number density is shown to have a minor influence on D_{eff} (both number densities result in free-molecular flow), while other drivers can contribute to a notable change in D_{eff}, whether that is an increase (for greater porosity and gas temperature) or a decrease (for greater adsorption probability, residence time and saturation limit).

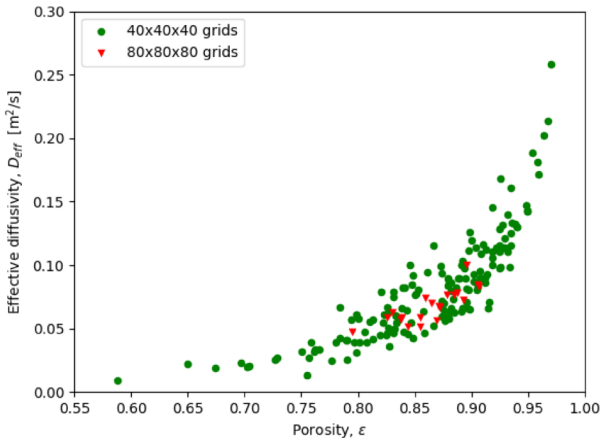

FIGURE 6. Effective diffusivity derivation for the mixed ceramic foam sample using the default configuration.

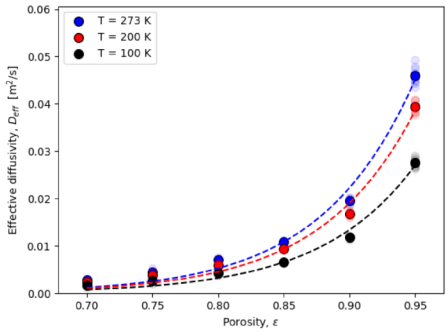

(a) Effective diffusivity trend when varying the gas temperature. The temperature shown is the initial gas temperature and the surface temperature.

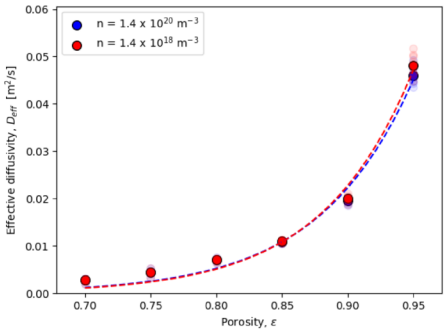

(b) Effective diffusivity trend when varying the gas number density.

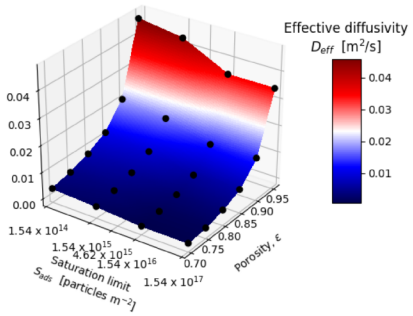

(c) Effective diffusivity surface plot when varying the porosity and saturation limit, with $\mathcal{P}_{\text{ads}} = 0.5$ and $\tau_{\text{ads}} = 10\ \mu$s.

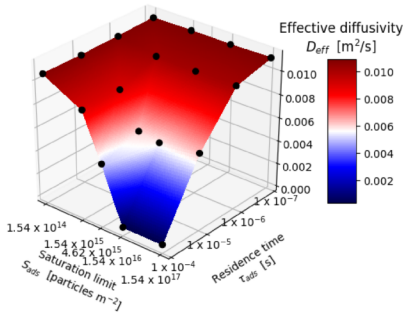

(d) Effective diffusivity surface plot when varying the residence time and saturation limit, with $\epsilon = 0.85$ and $\mathcal{P}_{\text{ads}} = 0.5$.

FIGURE 7. Effective diffusivity trends for the parametrised random porous media simulations. Mean values are denoted with an opaque filled circle, while individual DSMC simulations are represented with faded circles.

CONCLUSIONS

Derivation of the effective diffusivity in a DSMC framework has successively been laid out and verified for two benchmark cases. This was complemented by the further development of surface mechanisms of adsorption, desorption and saturation.

Application to highly porous geometries was considered, including those generated from μCT scans and those randomly generated from a python script. It is shown that taking a small subsample from a large μCT scan of a highly porous material is unlikely to give a porosity and tortuosity that is representative of the entire material and that a large number of subsamples must be studied to obtain reliable results.

The methodology to obtain the effective diffusivity of the mixed ceramic foam sample was presented and informative trends when temperature, gas number density, and adsorption parameters are varied are given using random porous media. This reveals useful information as the derivation of global medium quantities makes possible the use of simplified engineering methodologies that assume a homogeneous porous structure. Managing the interconnection of solid regions during the random generation of 3D porous media is left as future work.

ACKNOWLEDGMENTS

This work was developed under the ESA contract (4000115469/15/NL/KML/fg) with title Effect of a Regolith Liberated by a Rocket Plume Impingement. The authors would like to thank the National History Museum (London, UK) for providing the μCT scans.

REFERENCES

[1] S. Barraclough, A. Ratcliffe, R. Buchwald, H. Scheer, M. Chapuy, M. Garland, and D. Rebuffat, "Phootprint: A European Phobos Sample Return Mission," in *11th International Planetary Probe Workshop*, LPI Contributions, Vol. 1795 (2014) p. 8030.

[2] G. A. Bird, *Molecular gas dynamics and the direct simulation of gas flows* (Clarendon, Oxford, 1994).

[3] C. White, M. K. Borg, T. J. Scanlon, S. M. Longshaw, B. John, D. R. Emerson, and J. M. Reese, Computer Physics Communications **224**, 22–43 (2018).

[4] *hyStrath* Github repository, https://github.com/vincentcasseau/hyStrath/ (June 2018), commit ccca2dc.

[5] A. Einstein, *Investigations on the Theory of the Brownian Movement* (Dover, New York, 1926).

[6] J. M. Zalc, S. C. Reyes, and E. Iglesia, Chemical Engineering Science **59**, 2947–2960 (2004).

[7] C. White *et al.*, "Numerical and Experimental Capabilities for Studying Rocket Plume-Regolith Interactions," in *Proceedings of the 30th Rarefied Gas Dynamics Conference* (AIP, Victoria BC, Canada, July 10-15, 2016).

[8] C. White, T. J. Scanlon, and R. E. Brown, Journal of Spacecraft and Rockets **53** (2016).

[9] J. J. Telega and W. R. Bielski, Computers and Geotechnics **30**, 271–288 (2003).

[10] S. Chapman and T. G. Cowling, in *The Mathematical Theory of Non-uniform Gases* (Cambridge University Press, Cambridge, UK, 1970) 3rd ed.

[11] K. Koura and H. Matsumoto, Physics of fluids. A, Fluid dynamics **3**, 2459–246512 (1991).

[12] C. White, T. J. Scanlon, J. A. Merrifield, K. Kontis, T. Langener, and J. Alves, "Numerical and Experimental Capabilities for Studying Rocket Plume-Regolith Interactions," Tech. Rep. (2017).